Journal of Solid State Chemistry 185 (2012) 25–30

Contents lists available at SciVerse ScienceDirect

Journal of Solid State Chemistry

journal homepage: www.elsevier.com/locate/jssc

Electronic structure and anisotropic chemical bonding in TiNF from ab initio study

Samir F. Matar*

CNRS, Université de Bordeaux, ICMCB, 87 avenue du Dr Albert Schweitzer. 33600 Pessac, France

ARTICLE INFO

Article history:
Received 4 August 2011
Received in revised form
12 October 2011
Accepted 24 October 2011
Available online 4 November 2011

Keywords:
Nitride-fluoride
DFT
Semi-conducting
Iono-covalent bonding

ABSTRACT

Accounting for disorder in anatase titanium nitride fluoride TiNF is done through atoms re-distributions based on geometry optimizations using ultra soft pseudo potentials within density functional theory DFT. The fully geometry relaxed structures are found to keep the body centering of anatase ($I4_1/amd$ No. 141). The new structural setups are identified with space groups I-4m2 No. 119 and Imm2 No. 44 which obey the "group to subgroup" relationships with respect to anatase. In the ground state Imm2 structure identified from energy differences, TiNF is found semi-conducting with similar density of states features to anatase TiO_2 and a chemical bonding differentiated between covalent like Ti-N versus ionic like Ti-F. Inter-anion N-F bonding is also identified.

1. Introduction

Considering the iso-electronic relationship for valence shell states whereby 2 O ($2s^2$, $2p^4$)→N ($2s^2$, $2p^3$)+F ($2s^2$, $2p^5$), nitride-fluorides of formulation $A^{IV}NF$ type can be considered as "pseudo-oxides", iso-electronic of $A^{IV}O_2$ where A^{IV} is a generic tetravalent element. A few nitride-fluorides exist such as Mg_2NF [1] and ZrNF [2] and hypothetic SiNF was proposed by us from *ab initio* as a candidate of mixed-anions compound with potential properties such as anisotropic electric conduction, optical anisotropy [3]. Transition metal tetrahydrides $A^{IV}H_4$ with A=Ti through Ni, are also iso-electronic of $A^{IV}O_2$ and $A^{IV}NF$, they are known as molecular metals, such as "molecular titanium" TiH_4 [4].

Preparation and structural parameters of TiNF were provided in a short note by Wüstefeld et al. [5]. The synthesis protocol used temperature activated ammonolysis of $(NH_4)_2TiF_6$ fluoride and the x-ray refinement of the structure was done in $I4_1/amd$ space group (SG) of anatase TiO_2. The first column of Table 1 gives the experimental lattice parameters and the atomic positions of Ti and anionic positions shared by N and F [5]. Ti is expected to form covalent bonds with nitrogen and ionic bonds with fluorine due to the differences of electronegativity $\chi_{Ti}=1.54$, $\chi_N=3.04$ versus $\chi_F=3.98$ (while $\chi_O=3.44$). The chemical bonding mismatch is likely to generate different lattice distances, subsequent atomic disorder and original physical properties. For the purpose of studying these properties resolved at the atomic level, we provide herein an alternative description of the structure and atomic distribution assuming order and disorder within the anionic sublattice while preserving the experimental I centering within group to subgroup structural relationships. This is achieved through geometry optimizations based on energy criteria for determining the structure and atomic positions as well as a detailed description of the electronic band structure, density of states (DOS) and chemical bonding properties in the framework of the density functional theory (DFT) [6]. Computations in this framework have proven their validity not only for interpreting physical and chemical observables at the atomic scale, but also as a powerful predictive tool of new stoichiometry and materials [3,7] prior to their syntheses.

2. Computational details

Two computational methods built within the DFT were used, namely with use of pseudo potentials within the Vienna Ab-initio Simulation Package (VASP) package [8] for the geometry optimization and with all electrons computations within the augmented spherical wave method (ASW) [9] for an account of the chemical bonding properties.

In the VASP code, the ion-electrons interactions are treated by ultra-soft pseudo potentials (US-PP) according to Vanderbilt [10] whereas the electron-electron interaction is described in the local density approximation (LDA) [11]. Preliminary tests with the GGA gradient approximation [12] led to overestimated volumes versus experiment (cf. Table 1 GGA columns). The use of pseudo-potentials allows a considerable reduction of the necessary number of plane waves per atom for transition metals (here Ti)

* Fax: +33 5 4000 27 61.
E-mail address: matar@icmcb-bordeaux.cnrs.fr

0022-4596/$ - see front matter © 2011 Elsevier Inc. All rights reserved.
doi:10.1016/j.jssc.2011.10.041

Table 1
TiNF: Geometry optimized structures obeying the group-subgroup relationships and experimental anatase in first column.

TiNF	Exp. [5]	Hypo. 1		Hypo. 2	
		LDA	GGA	LDA	GGA
a/b (Å)	3.789	3.851	3.890	3.807/3.810	3.869/3.870
c (Å)	9.486	9.547	9.875	9.656	9.931
Volume (Å^3)	136.20	141.58	149.82	140.70	148.69
Ti1	0, 0, 0 (4*a*)	0, 0, 0 (2*a*)	0, 0, 0 (2*a*)	0, 0, 0.025 (0, 0, z) (2*a*)	0, 0, 0.027 (0, 0, z) (2*a*)
Ti2	0, 1/2 1/4	0, 1/2, 1/4 (2*c*)	0, 1/2, 1/4 (2*c*)	0, 1/2, 0.275 (0, 1/2, z′) (2*b*)	0, 1/2, 0.277 (0, 1/2, z′) (2*b*)
N1	0, 0, u (u=0.2083) (8*e*)	0, 1/2, *z* (*z*=0.051) (4*f*)	0, 1/2, *z* (*z*=0.055) (4*f*)	0, 0, 0.211(0, 0, z) (2*a*)	0, 0, 0.210 (0, 0, z) (2*a*)
N2	0, 0, -u	0, 1/2, −z	0, 1/2, −z	0, 1/2, 0.461 (0, 1/2, z′) (2*b*)	0, 1/2, 0.460 (0, 1/2, z′) (2*b*)
F1	0,1/2,u+1/4	0, 0, *z*′ (*z*′=0.225) (4*e*)	0, 0, *z*′ (*z*′=0.226) (4*e*)	0, 0, 0.764(0, 0, z) (2*a*)	0, 0, 0.763 (0, 0, z) (2*a*)
F2	0,1/2, u−1/4	0, 0, −*z*′	0, 0, −*z*′	0, 1/2, 0.015 (0, 1/2, z′) (2*b*)	0, 1/2, 0.013 (0, 1/2, z′) (2*b*)
Symmetry operations	**16**: 1E, 1I, 5R2, 5M, 2R2, 2S4	**8**: 1 E, 3 R2, 2M, 2S4	**8**: 1 E, 3 R2, 2M, 2S4	**4**: 1 E, 1 R2, 2 M (M_x, M_y)	**4**: 1 E, 1 R2, 2 M (M_x, M_y)
Space group	$I4_1/amd$ No. 141	I-4*m*2 No. 119	I-4*m*2 No. 119	I*mm*2 No. 44	I*mm*2 No. 44
Energy (eV)	–	−51.38	−47.32	−52.58	−48.68

and first row elements (such as N, O and F), thus force and full stress tensor can be calculated and used to relax atoms into their ground state. The conjugate-gradient algorithm [13] is used in this computational scheme to relax the ions of the different structural setups of TiNF. The calculations were performed with an energy cut-off of 425 eV for the plane wave basis set. The tetrahedron method with Blöchl corrections [14] as well as a Methfessel-Paxton [15] scheme were applied for both geometry relaxation and total energy calculations. Brillouin-zone (BZ) integrals were approximated using the special k-point sampling of Monkhorst and Pack [16]. A large number of 150 k-points were used in the irreducible wedge of the body centered tetragonal and orthorhombic (*vide infra*) BZ to perform total energy calculations. The optimization of the structural parameters was performed until the forces on the atoms were less than 0.02 eV/Å and all stress components less than 0.003 eV/Å^3.

Subsequent all-electron calculations for a detailed analysis of the electronic band structure and particularly the properties of chemical bonding were performed using the full potential scalar-relativistic augmented spherical wave (ASW) method [9]. In the ASW method, the wave function is expanded in atom-centered augmented spherical waves, which are Hankel functions and numerical solutions of Schrödinger's equation, respectively, outside and inside the so-called augmentation spheres. In the minimal ASW basis set, we chose the outermost shells to represent the valence states and the matrix elements were constructed using partial waves up to $l_{max}+1=3$ for Ti and $l_{max}+1=2$ for N and F. Low energy lying F(2*s*) were considered as core states. In order to optimize the basis set, additional augmented spherical waves are placed at carefully selected interstitial sites (IS). Self-consistency was achieved when charge transfers ΔQ and energy changes ΔE between two successive cycles were such as: $\Delta Q < 10^{-8}$ and $\Delta E < 10^{-6}$ eV. The BZ integrations were performed using the linear tetrahedron method within the irreducible wedge [14].

The relative magnitude of the chemical bonding is obtained based on the overlap population analysis: S_{ij} (i, j two chemical species). The crystal orbital overlap population (COOP) criterion is used [17] as implemented within the ASW method [9]. In the plots positive, negative and zero COOP magnitudes indicate bonding, anti-bonding and non-bonding interactions respectively. Here we use the COOP criterion to address relative bonding intensities and positions. We note that other schemes for describing the chemical bonding such as those based on both the overlap and the Hamiltonian populations (ECOV: covalent bond energy) are also accessible within the ASW method. They provide similar qualitative results to the COOP.

3. Results and discussion

3.1. Geometry optimization and charge density

In the experimental anatase-like structure of TiNF [5], the replacement of the oxygen atoms by N and F can be done either by putting all N at $z=0$ planes and all F at $z=1/2$ planes (Hypo. 1) or by alternating N and F positions along c so that both atoms are found at $z=0$ and $z=1/2$ (Hypo. 2). The two hypotheses were tested with unrestricted geometry optimizations. It needs to be stressed that there must be a group to subgroup relationship between the initial SG and the final ones obtained by geometry optimizations [18].

With Hypo. 1 the full geometry relaxation keeps the cell tetragonal. The *I* centering is preserved but the number of operations decreases from 16 to 8 due to the dispatching of the atoms from four-fold to two fold Wyckoff positions for Ti and from one eight-fold (N/F) to two four-fold Wyckoff positions for N and F respectively. The results are given in 2nd column of Table 1. Their analysis leads to assign the *I*-4*m*2 SG which is a subgroup of $I4_1/amd$. The other subgroups are *Fddd*, *Imma*, $I4_1/a$, $I4_122$, $I4_1md$ and *I*-42*d*, however they were not obtained from the geometry optimizations. The volume is calculated slightly larger than the experimental value due to the increase of both a and c cell constants but the initial cell proportions are kept. Similar results are obtained for the calculations using the GGA exchange-correlation functional but the volume is much larger. The structure sketched in Fig. 1b is distorted with respect to the experimental one as it can be seen from the distances (Fig. 1a). The order within the anionic sublattices N and F can be viewed as a succession of (Ti/N), (Ti/F), (Ti/N) etc. layers along the tetragonal *c*-axis.

For Hypo. 2 atomic distributions, a further lowering of the number of symmetry operations from 8 (*I*-4*m*2 SG, Hypo. 1) to 4 is obtained after structural optimization. The symmetry analysis leads to I*mm*2 SG which is a subgroup of *I*-4 *m*2. The other subgroups are *F222*, *I-4*, *P-4m2* and *P-4n2*, however they could not be obtained from the geometry optimizations. The atoms are all found in 2*a* and 2*b* Wyckoff positions as shown in Table 1. I*mm*2 SG is orthorhombic but a and b magnitudes of the lattice parameters are very close so that the lattice can be assimilated to a body centered tetragonal, like anatase. The volume is close to the one calculated with Hypo. 1 and the cell proportions are preserved but the energy is lowered by 1.2 eV, leading to propose Hypo. 2 model as the ground state. The same energy trend is observed for the GGA based calculations, i.e., with a large stabilization of the compound in Hypo. 2 configuration. The resulting structure sketched in Fig. 1c with characteristic

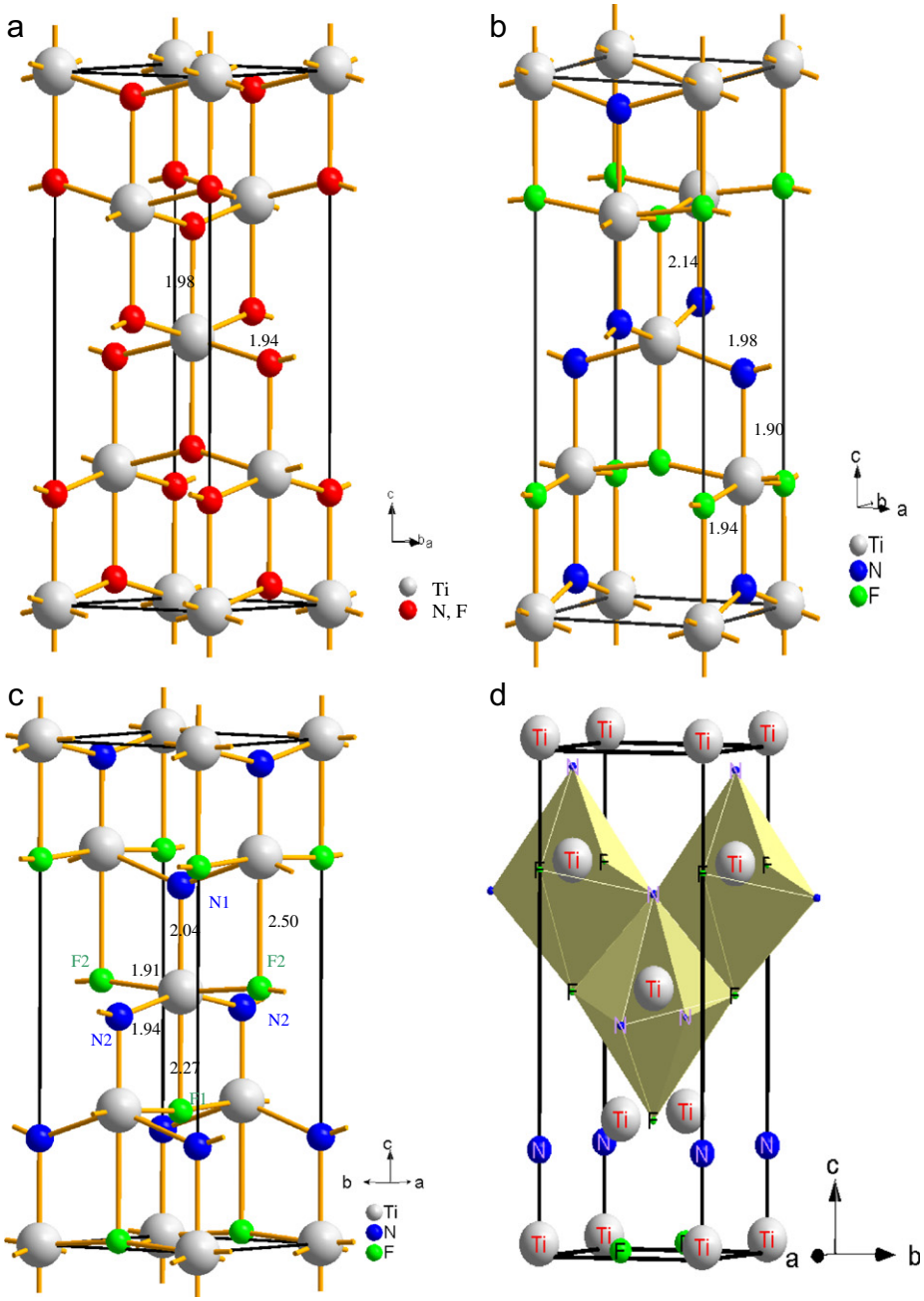

Fig. 1. TiNF structure representations with characteristic Ti-N and Ti-F distances in Å units; (a) Experimental anatase TiNF structure with random N/F distribution; (b) geometry optimized structure with ordered N/F distribution (Hypo. 1); (c) geometry optimized structure with disordered N/F distribution (Hypo. 2); (d) Hypo. 2: corresponding arrangement of open faceted *TiN3F3* distorted octahedra.

distances shows a larger distortion with respect to Hypo. 1 structure (Fig. 1b) as it can be seen from the scattering of distances between Ti on one hand and N and F on the other hand. Yet it resembles the anatase structure (Fig. 1a) but the disorder leads to a succession of (Ti/N/F), (Ti/F/N), (Ti/N/F) etc. layers along the c-axis. The structure is reproduced in Fig. 1d to show the stacking of the distorted edge sharing *TiN3F3* octahedra. The configuration of these octahedra resembles one of the two isomers encountered in the chemistry of inorganic complexes, namely the "meridianal" one. The other possibility of "facial" conformation is not obtained here. This is because of the symmetry related positions in the structure: N1 (2a) is opposite to F1 (2a) along the *c*-axis and N2-N2 (both at 2b) and F2-F2 (both at 2b) are equatorial; cf. Table 1. Any other configuration such as the one reproducing a facial isomer destroys the symmetry and leads to an unstable state.

From the electronegativity values above one expects charge transfer from Ti towards N and F with different amounts. In order to better assess this feature, we analyzed the charge density issued from the self consistent calculations using the Bader AIM (Atoms in Molecules Theory) approach [19]. The resulting charges Ti: +2.34; N: −1.50; F: −0.84 show the expected trend of charge transfer from Ti to N and F. Compared to the rule of thumb view of fully ionized chemical species for tetravalent titanium (Ti^{4+}), trivalent nitrogen (N^{3-}) and monovalent fluorine (F^{1-}), the anionic character for fluorine is larger (84%) than for nitrogen (50%) in agreement with their respective ionic and covalent characters.

3.2. Electronic band structure

The electronic structure and the chemical bonding properties are calculated with the optimized lattice parameters. With the ASW method one starts from neutral atoms. At self consistency there is charge redistribution between the atomic species and the charge transfer is actually observed from Ti to N, F in agreement with the Bader charge analysis above. Interstitial spheres, IS, receive charge residues. Further the band structure will be shown to provide an illustration for the expected chemical picture of the nitride fluoride.

For the sake of confronting the two electronic structures according to Hypo. 1 and Hypo. 2, the site projected DOS (PDOS) accounting for site multiplicity are shown for both in Fig. 2. For Hypo. 1 the energy reference along x abcissa axis is at the Fermi level (E_F) (Fig. 2a). This is because there is a finite PDOS arising from Ti PDOS while the N and F PDOS are at a minimum leading to assign a metallic behavior to the compound in Hypo. 1 configuration. The valence band VB is divided into three main blocks pertaining to: N($2s$) around -14 eV then F ($2p$) in the range $\{-5.5, -7$ eV$\}$ and N ($2p$) in the range $\{-4.8$ eV, $E_F\}$. The mixing between these valence states and Ti ones is clear from the presence of Ti PDOS under all three of them.

On the contrary in Fig. 2b of ground state Hypo. 2 DOS, the energy reference along x is at E_V, top of the VB, separated from the conduction band (CB) by a band gap of $\sim$2 eV. The CB is dominated by Ti d states due to their small filling already in the atomic state, Ti belonging to the beginning of the 3d period. The compound is then insulating. However we do not expect band gaps to be correctly obtained with the used approximation for exchange and correlation due to the overbinding character of the LDA. For the sake of clarity we do not show small contribution PDOS arising from IS. The lower part of the valence band (VB) is dominated by N($2s$) at~ -12 eV then F($2p$) in the range $\{-7, -5$ eV$\}$ and N($2p$) in the range $\{-5, 0$ eV$\}$, i.e. up to E_V. Similar to Fig. 2a of Hypo. 1 DOS, the Ti PDOS intensities below the two p blocks point to Ti-N as well as Ti-F mixing. This is addressed in the analysis of the chemical bond in next section. Due to their belonging to two different lattice sites and interatomic distances (Table 1, Hypo. 2 column) Ti1/Ti2, N1/N2 and F1/F2 PDOS exhibit slight energy shift but without change of the main PDOS blocks.

Fig. 2c shows the PDOS of anatase TiO_2 calculated for the sake of comparison. Like above the compound is insulating and large similarities with TiNF are observed. The VB shows that O($2s$) are found at lower energy (-16 eV) than N (2 s) at -12 eV (in upper panel). Keeping in mind the F ($2s$) found at very lower energy, the observations are in agreement with the electronegativity trend between the elements, i.e. $\chi_N < \chi_O < \chi_F$. The other difference with respect to TiNF, is that O($2p$) band extends over 5 eV, i.e. twice broader than the two well separated p blocks in TiNF. This features a dismutation-like behavior known for cations and resembled here by replacing O by a more covalent element (N) on one hand and by a more ionic one (F) on the other hand.

The band dispersions along major lines of tetragonal Brillouin zone are presented in Fig. 3 for the ground state structure. Reproducing the DOS (Fig. 2) on the right hand side shows that

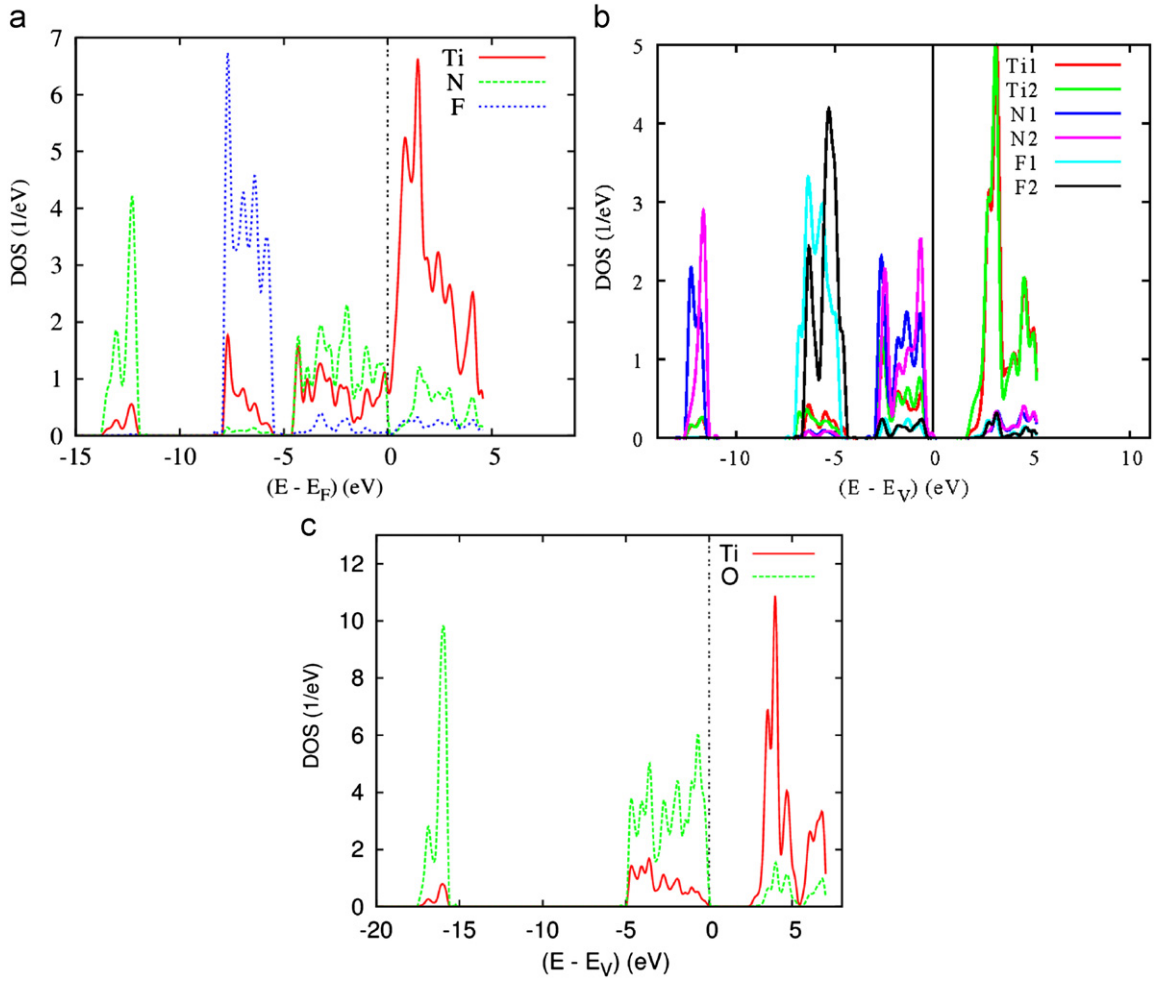

Fig. 2. Site projected DOS for anatase derived TiNF in (a) Hypo. 1, (b) Hypo. 2 and (c) anatase TiO_2.

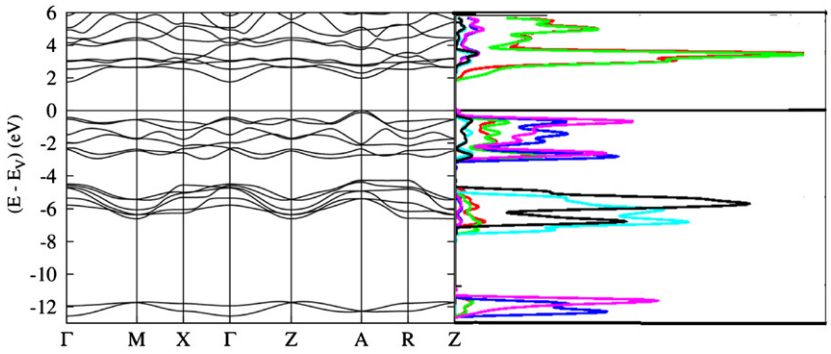

Fig. 3. Band structure of TiNF in anatase derived structure (Hypo. 2) and corresponding DOS.

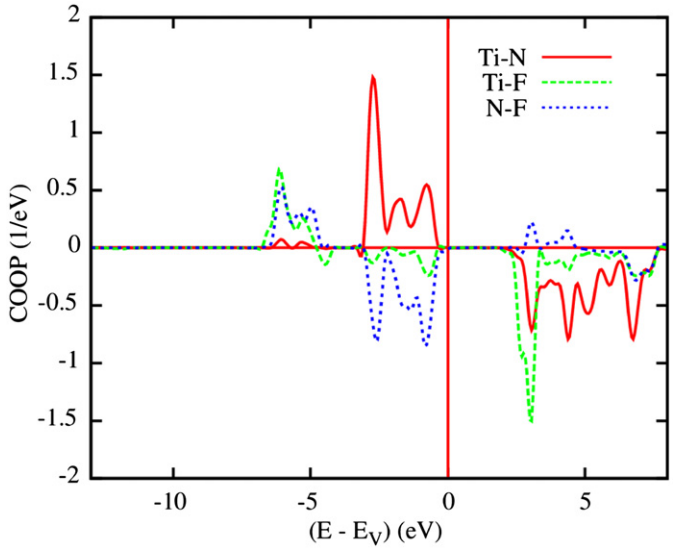

Fig. 4. Chemical bonding in anatase derived TiNF (Hypo. 2) from crystal orbital overlap population (COOP) analysis.

the band structure mirrors them with the band gap and the relative positions of the PDOS blocks. It also allows assigning an indirect band gap between X_{VB} and Γ_{CB}. The band gap magnitude of ~2 eV is close to that found for N-doped anatase TiO_2 [20] while anatase TiO_2 has a band gap of 3.2 eV [21]. Its reduction is likely due to the covalence brought by nitrogen. This is also obtained from nitriding magnesium fluoride to produce nitride fluorides, leading to a steady decrease of the band gap from 7 eV (MgF_2) to ~2 eV (Mg_2NF) [22].

3.3. Chemical bonding

The bonding within the valence band VB is mainly found between titanium on one hand and the anionic sublattices on the other hand. Because of the feature of edge sharing octahedra (Fig. 1d) there should be non negligible N-F interactions besides Ti-N and Ti-F. The pair interactions are accounted for with the crystal orbital overlap populations (COOP) analysis given in Fig. 4. Positive, negative and zero COOP correspond to bonding, antibonding and non-bonding interactions respectively. Using a gross definition, the COOP are the DOS weighted by the overlap integral S_{ij}. They have the same inverse energy (1/eV) unit as the DOS. For the sake of clear presentation the different sites are regrouped for a single chemical species. Below −6 eV where N(2*s*) states are found in Fig. 2b, there is no bonding due to the non directional character of *s* states. There are two main bonding areas within the VB, in the energy ranges {−6,−5 eV} with dominant Ti-F and from −3 eV up to E_V for Ti-N, corresponding to the energy positions of F (2*p*) and N (2*p*) PDOS respectively (Fig. 2b). They are of bonding character (positive COOP magnitudes) throughout the VB; antibonding counterparts are observed within the CB. The Ti-N COOPs have larger magnitude than Ti-F ones due to the smaller overall Ti-N distances and to the covalent T-N bonding character. N-F COOP are bonding in the {−7,−5 eV} energy window and antibonding from −3 eV up to E_V where N states become involved with the bonding with Ti *d* ones. Due to the small filling of Ti states, the extra electrons arising from N and F are found in bonding states. This is contrary to the N-F interaction which becomes strongly antibonding near the top of the VB although it is of bonding character in the lower part of the VB. This is equally assessed due to the larger filling of F states and to the half filled N ones. Then this interaction is not stabilizing for the compound, contrary to bonding Ti-N and Ti-F.

4. Conclusions

In this work an original approach of the experimental structure of anatase TiNF has been provided with the objective of addressing the atom resolved electronic band structure and the properties of chemical bonding. Based on anatase structure, two different ordering scheme models were considered and geometry optimized yielding new structures obeying the group→subgroup relationships:

$I4_1/amd$ N°141 (exp.)→$I\bar{4}m2$ N°119→$Imm2$ N°44.

The ground state with *Imm*2 SG is a distorted anatase structure. It is found semi-conducting with similar density of states to anatase TiO_2. The chemical bonding is differentiated between covalent like Ti-N versus ionic like Ti-F, stronger for the former. Such anisotropic bonding properties are likely to generate peculiar physical properties. Their investigations are underway.

Dedication

This paper is dedicated to Ziad Doumit and Alain Essayan.

Acknowledgments

Discussions with and critical reading of the manuscript by Dr. Volker Eyert of Materials Design Co. are gratefully acknowledged.

References

[1] H. Seibel, T.R. Wagner, J. Solid State Chem. 177 (2004) 2772.
[2] X. Chen Zhu, S. Yamanaka, Solid State Comm 130 (2004) 227.

[3] E. Betranhandy, S.F. Matar, Phys. Rev. B 72 (2005) 205108.
[4] D.M. Hood, R.M. Pitzer, H.F. Schaefer, J. Chem. Phys. 71 (1979) 705.
[5] C. Wüstefeld, Th. Vogt, U. Löchner, J. Strähle, H. Fuess, Angew. Chemie Int. Ed. in English 27 (1988) 929.
[6] W. Kohn, L.J. Sham, Phys. Rev. A 140 (1964) 1133;
P. Hohenberg, W. Kohn, Phys. Rev. B 136 (1965) 864.
[7] S.F. Matar, G. Demazeau, J. Solid State Chem. 183 (2010) 994.
[8] G. Kresse, J. Hafner, Phys. Rev. B 47 (1993) 558;
G. Kresse, J. Hafner, Phys. Rev. B 49 (1994) 14251;
G. Kresse, J. Furthmüller, Comput. Mater. Sci. 6 (1996) 15;
G. Kresse, J. Furthmüller, Phys. Rev. B 54 (1996) 11169.
[9] A.R. Williams, J. Kübler, C.D. Gelatt Jr., Phys. Rev. B 19 (1979) 6094;
V. Eyert, The Augmented Spherical Wave Method–A Comprehensive Treatment, Lecture Notes in Physics, Springer, Heidelberg, 2007.
[10] D. Vanderbilt, Phys. Rev. B 41 (1990) 7892.
[11] D.M. Ceperley, B.J. Alder, Phys. Rev. Lett. 45 (1980) 566.
[12] J. Perdew, K. Burke, M. Ernzerhof, Phys. Rev. Lett. 77 (1996) 3865.
[13] W.H. Press, B.P. Flannery, S.A. Teukolsky, W.T. Vetterling, Numerical Recipes, Cambridge University Press, New York, 1986.
[14] P.E. Blöchl, Phys. Rev. B 50 (1994) 17953.
[15] M. Methfessel, A.T. Paxton, Phys. Rev. B 40 (1989) 3616.
[16] H.J. Monkhorst, J.D. Pack, Phys. Rev. B 13 (1976) 5188.
[17] R. Hoffmann, Angew. Chem. Int. Ed. Engl. 26 (1987) 846.
[18] M.I. Aroyo, J.M. Perez-Mato, C. Capillas, E. Kroumova, S. Ivantchev, G. Madariaga, A. Kirov, H. Wondratschek., Z. für Kristallog 221 (2006) 15.
[19] R. Bader, Chem. Rev. 91 (1991) 893.
[20] L. Wan, J.F. Li, J.Y. Feng, W. Sun, Z.Q. Mao, Materials Science and Engineering B 139 (2007) 216.
[21] Bin LIAO, Li-Zhao QIN, Xian-Ying WU, Xing-Gang HOU, An-Dong CHENG Ken LIU, Chinese J. Struct. Chem. 28 (2009) 869.
[22] C.M. Fang, K.V. Ramanujachary, H.T. Hintzen, G. de With, J. Alloys, and Compounds 351 (2003) 72.